Memristive switching mechanism for metal/oxide/metal nanodevices

J. JOSHUA YANG, MATTHEW D. PICKETT, XUEMA LI, DOUGLAS A. A. OHLBERG, DUNCAN R. STEWART* AND R. STANLEY WILLIAMS

Hewlett-Packard Laboratories, Palo Alto, California 94304, USA
*e-mail: duncan.stewart@hp.com

Nanoscale metal/oxide/metal switches have the potential to transform the market for nonvolatile memory and could lead to novel forms of computing. However, progress has been delayed by difficulties in understanding and controlling the coupled electronic and ionic phenomena that dominate the behaviour of nanoscale oxide devices. An analytic theory of the 'memristor' (memory-resistor) was first developed from fundamental symmetry arguments in 1971, and we recently showed that memristor behaviour can naturally explain such coupled electron–ion dynamics. Here we provide experimental evidence to support this general model of memristive electrical switching in oxide systems. We have built micro- and nanoscale TiO$_2$ junction devices with platinum electrodes that exhibit fast bipolar nonvolatile switching. We demonstrate that switching involves changes to the electronic barrier at the Pt/TiO$_2$ interface due to the drift of positively charged oxygen vacancies under an applied electric field. Vacancy drift towards the interface creates conducting channels that shunt, or short-circuit, the electronic barrier to switch ON. The drift of vacancies away from the interface annilihilates such channels, recovering the electronic barrier to switch OFF. Using this model we have built TiO$_2$ crosspoints with engineered oxygen vacancy profiles that predictively control the switching polarity and conductance.

Existing materials and technologies in the semiconductor industry are approaching their physical limits, and technology breakthroughs in materials and device concepts are required as device sizes continuously decrease[1]. Developing nanoscale memory-bit cells[2,3] for nonvolatile random access memory (NVRAM) is one key technological step that is necessary to extend the functional equivalent of Moore's law[4] for Boolean computing. Ultrahigh-density analogue resistive memory cells (RRAM) may also enable a new era of non-Boolean neuromorphic computing[5,6].

Metal oxides have attracted significant attention as the insulating layer in metal/insulator/metal crosspoint cells for RRAMs and NVRAMs[7] because of their wide range of electrical properties—most are wide-bandgap semiconductors susceptible to doping by a variety of defects and impurities. Many are intrinsically 'self-doped' by native interstitial or vacancy point defects. Consequently, the mechanism for metal-oxide-based resistive switches is still a matter of debate. Different models have been suggested, including alteration of the bulk insulator resistivity using defects or trapped carriers[8–16], modification of the metal/insulator interface resistivity, also with defects or trapped carriers[17–23], or the formation of localized metal-atom chains that bridge the electrode materials under an electric field[24,25].

It is possible that several different mechanisms may co-exist, and different mechanisms could be dominant in different materials systems[7]. This uncertainty is exacerbated by the great difficulty in characterizing the physical changes responsible for the electrical switching, because the active regions of the devices are extremely small and buried under a metal contact. Here we manipulate and ultimately engineer the device structure to reveal that the mechanism for TiO$_2$ switching is the shunting and recovery of the metal/oxide interfacial electronic barrier caused by the localized drift of oxygen vacancies.

SWITCHING BEHAVIOUR

A promising switching behaviour we have observed in both micrometre- and nanoscale crosspoint devices is the bipolar, reversible and nonvolatile switching of Pt/TiO$_2$/Pt structures with ON/OFF conductance ratios of $\sim 1 \times 10^3$. Figure 1a presents an atomic force microscopy (AFM) image of crosspoint nanodevices with a 50-nm-thick TiO$_2$ insulator sandwiched between 50-nm-wide top and bottom Pt nanowire electrodes fabricated by nanoimprint lithography[26,27].

For electrical testing, we applied a bias voltage to the top electrode, with the bottom electrode grounded for all measurements in this study. The initial current–voltage ($I-V$) curve of the device in its virgin (pre-switching) state exhibits a rectifying characteristic (Fig. 1b). After a single irreversible forming step (see Methods), the multiple switching $I-V$ curves (red lines) in Fig. 1c demonstrate a high degree of repeatability. Lower current and voltage drive (blue line) reveals multiple resistive states of the device. The device was switched ON only by applying a negative bias and OFF only by applying the opposite (positive) bias (this is the definition of a bipolar switch). This switching polarity was defined by the device fabrication procedure and was independent of the voltage bias polarity of the forming step, which induces a profound and essentially permanent change to the oxide film by means of electroreduction[28]. The switching speed at high bias voltages was measured to be less than 50 ns. These electrical characteristics were reproduced in more than 100 crosspoint devices built on more than 20 different wafers. The $I-V$ trace (Fig. 1c) of the device in the ON
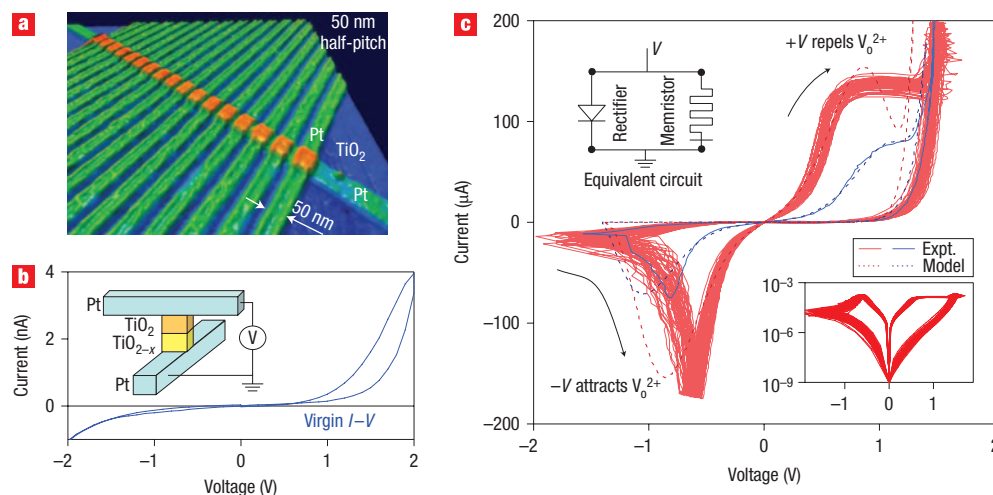
Figure 1 Bipolar reversible and nonvolatile switching of nanoscale TiO$_{2-x}$ devices. a, An AFM image of 1×17 nano-crosspoint devices with 50 nm half-pitch. Pt nanowires fabricated by nanoimprint lithography sandwich a 50-nm-thick TiO$_2$ insulating thin film. **b**, The initial $I-V$ curve of the device in its virgin (pre-switching) state exhibits a rectifying characteristic. Inset: The 50-nm TiO$_2$ has two constituent layers; a near-stoichiometric TiO$_2$ layer rests on top of an oxygen-deficient TiO$_{2-x}$ layer (see text). All electrical voltages were applied with the lower nanowire electrode grounded. **c**, Experimental (solid) and modelled (dotted) switching $I-V$ curves. The red curves represent 50 experimental switching loops traversed as figure-of-eights, which show a high degree of repeatability. The blue curve is a lower current experimental switch loop that demonstrates the multiple resistive states of the device. The $I-V$ trace of the device in the ON state exhibits a symmetric sinh-like curve, and the OFF state shows an asymmetric rectifying curve similar to the virgin state. Lower inset: The log-scale switching $I-V$ curves show ON/OFF conductance ratios of $\sim 1 \times 10^3$. Upper inset: The equivalent circuit model consists of a rectifier in parallel with a memristor. The memristor symbol is modified here with a bar to indicate its polarity. A positive bias applied to the end of the memristor with the bar switches it ON; that is, with this bias polarity the resistance of the memristor decreases. This memristor + rectifier circuit model, implemented as equation (1), yields the dotted lines (V_o: Oxygen vacancy).

state was an exponential function in both quadrants, well fit by the form $I \approx \beta \sinh(\alpha V)$, which is often characteristic of electron tunnelling (α and β are fitting constants). In the OFF state the $I-V$ curve was rectifying, similar to the virgin state.

These $I-V$ curves contain valuable information for deciphering the nature of the ON and OFF states. For instance, the rectification suggests that the OFF state may be limited by Schottky-like transport at one of the metal/oxide interfaces. However, for the thin-film device structure of Fig. 1, the top and bottom interfaces of the device cannot be isolated for electrical characterization before or after a switching event, and thus it is not possible to identify the separate role of each interface. Therefore, a new experimental design that enables the junction interfaces to be studied separately is needed to obtain better insight into the switching.

Single-crystalline TiO$_2$ was used to elucidate how the metal/oxide interfaces control the device resistance. As shown in Fig. 2a, a single crystal of rutile TiO$_2$ (bandgap $E_g \approx 3.0$ eV) was first annealed in a 95% N$_2$ and 5% H$_2$ gas mixture at 550 °C for 2 h to create an oxygen-deficient layer near the surface. Oxygen vacancies in TiO$_2$ are known to act as n-type dopants[29], transforming the insulating oxide into an electrically conductive doped semiconductor (see Supplementary Information, Figs S1–S4, for detailed physical characterization of the TiO$_2$ single crystal and thin films). Metal/semiconductor contacts are typically ohmic in the case of very heavy doping, and rectifying (Schottky-like) in the case of low doping[30]. We deposited two pairs of 100 μm × 100 μm Pt and Ti electrode contact pads onto the single crystal, as shown schematically in Fig. 2a: pads 1 and 4 were Pt films (80 nm thick) and pads 2 and 3 were Ti films (5 nm thick) with Pt (80 nm thick) caps. The 5-nm Ti layer was used as a chemically reactive contact to further reduce the TiO$_2$ and create a locally high concentration of oxygen vacancies close to the metal/semiconductor interface. The four-probe electrical measurement

between these two Ti pads showed a ~ 40 Ω resistance and a linear $I-V$ (labelled 2−3 in Fig. 2c), demonstrating that both interfaces were ohmic and the bulk resistance of the annealed single crystal was low. In contrast, the electrical resistance between the two chemically unreactive Pt contact pads 1 and 4 was four orders of magnitude higher, with a symmetric nonlinear $I-V$ characteristic (labelled 1−4 in Fig. 2c). The $I-V$ characteristic between unmatched contacts 1 (Pt) and 3 (Ti) with pad 3 grounded (labelled 1−3$_{Gnd}$ in Fig. 2c) exhibited a rectifying characteristic similar to that observed for the nanoscale thin-film device of Fig. 1. Because the interface under pad 3 was known to be ohmic, and the rutile bulk resistivity was low, we directly infer that the electronic transport was controlled by a Schottky-like barrier under pad 1, that is, between the pure Pt contact and the n-type (reduced) rutile. The opposite polarity rectifying $I-V$ curve measured between pads 2 (Ti) and 4 (Pt) with pad 4 grounded (labelled 2−4$_{Gnd}$ in Fig. 2c) revealed a similar Schottky-like contact under pad 4. These measurements were confirmed by measuring all Pt−Ti two-terminal permutations.

As the energy diagram in Fig. 2b illustrates schematically, the high vacancy concentration under the Ti electrodes (and the lower Ti workfunction) serves to collapse the Schottky-like barrier and produce ohmic contacts, whereas the low vacancy concentration under the Pt pads maintains the Schottky-like barrier between Pt and TiO$_2$ to produce rectifying junctions. When the rutile single crystal was annealed further at a higher temperature and for a longer time (for example, 900 °C, 5 h) to increase the near-surface vacancy concentration, even the pure Pt contacts became ohmic. Comparing these data to the rectifying $I-V$ curves of the thin-film nanodevice in Fig. 1, we conclude that the top interface of the thin-film device is non-ohmic (maybe Schottky-like) and the bottom interface is ohmic-like for both the virgin state and the OFF switch state.
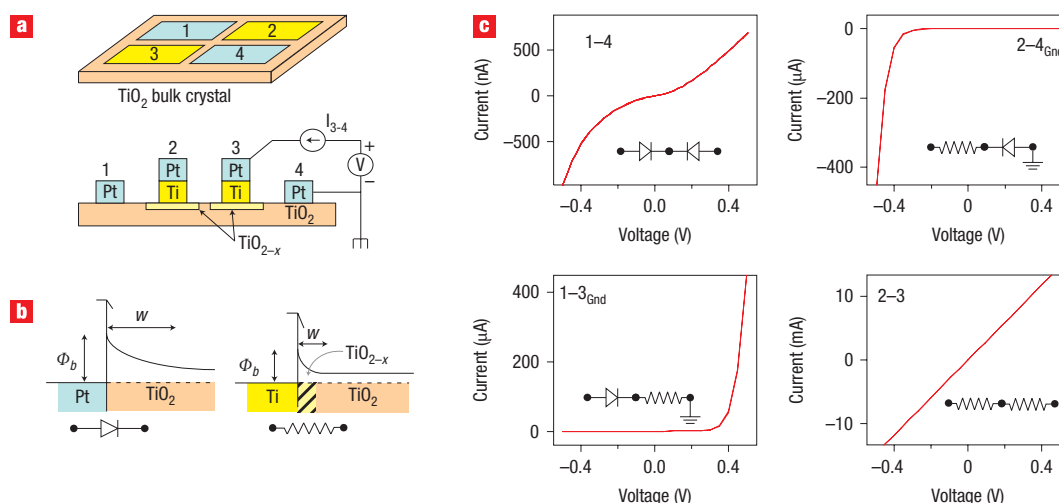
Figure 2 Junctions on single-crystal TiO$_2$ show the role of the interfaces in determining the electrical behaviour. a, Schematic of the electrodes and the single crystal. Four adjacent pads were deposited as pairs of Pt (blue) and Ti/Pt (yellow) contacts. **b**, Energy diagram showing the low oxygen vacancy concentration under the Pt pads maintaining the Schottky-like barrier (denoted by a rectifier) between Pt and TiO$_2$ to produce rectifying junctions, whereas the high vacancy concentration at the interfaces under the Ti/Pt pads collapses the Schottky-like barrier and produces ohmic contacts (denoted by a resistor). Φ_b and w are the electronic barrier height and width. **c**, The four-probe $I-V$ curves between the combinations of the four pads in **a**. The insets to these $I-V$ diagrams are the corresponding equivalent circuit diagrams consisting of two electronic elements (rectifier or resistor) in series.
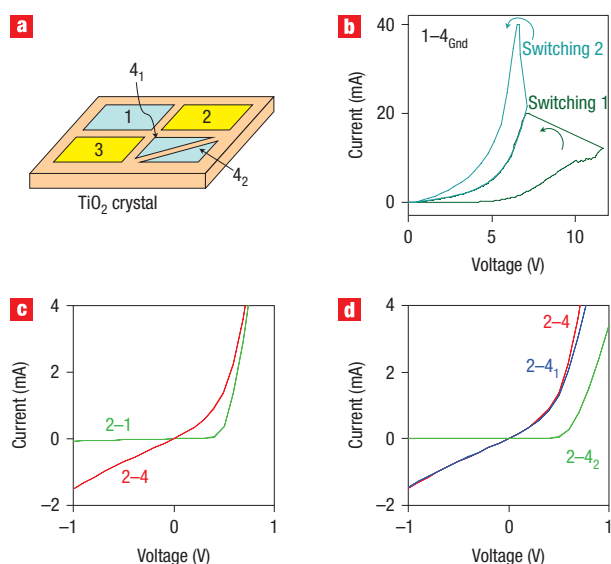

Figure 3 Switching is local and occurs at the Pt/TiO$_2$ interface.
a, Schematic of the junctions with the single-crystal TiO$_2$: pads 1 and 4 are Pt; pads 2 and 3 are Ti. After the initial measurements in **b**, pad 4 was cut in half. **b**, $I-V$ curves of two switching cycles between pad 1 and pad 4 with pad 4 grounded. **c**, The $I-V$ curves between pad 2 (grounded) and pad 1 and pad 4 after 'Switching 2', showing the change during switching occurs only under effectively negatively charged pad 4. **d**, Pad 4 was cut into two halves, 4_1 and 4_2 after Switching 2. The $I-V$ curves between pad 2 (grounded) and 4_1 and 4_2 demonstrate that the interface change under pad 4 is localized to the 4_1 part.

To explore the ON switch state, an increasing positive voltage bias was applied on Pt pad 1 with Pt pad 4 grounded until the device switched to a more conductive state, as shown by the 'Switching 1' curve in Fig. 3b. This switching was nonvolatile; a subsequent

voltage sweep ('Switching 2' curve) retraced the first high conductivity curve until the device switched to an even more conductive state. In order to determine whether the switching took place under the positively biased contact 1 or the (effectively) negatively biased contact 4, an $I-V$ curve for each was measured separately using the ohmic Ti contact 2. The $I-V$ curve measured between contacts 1 and 2 maintained the rectifying characteristic with very little change. However, as shown by the red curve in Fig. 3c, the rectifying behaviour of electrode 4 was dramatically reduced. Thus, only the Schottky-like barrier at the negatively biased interface was affected by the switching event. This can be explained by the fact that oxygen vacancies in TiO$_2$ are known to be positively charged and mobile[31]; the negatively biased electrode attracts the vacancies from the rutile crystal to the interface, causing a partial collapse of the Schottky-like barrier.

The question that remains is whether the change at the interface under contact 4 is uniform or localized, as some researchers[2,32] have observed the formation of localized regions of high conductance under a contact to a switched metal oxide. To investigate this issue, pad 4 was cut into two halves, denoted 4_1 and 4_2 in Fig. 3a. The $I-V$ curves between ohmic Ti pad 2 and these two Pt half-pads are presented in Fig. 3d to compare them with the $I-V$ curve (in red) between pad 2 and the uncut pad 4. This shows that the interface change was localized under pad 4_1, because the $I-V$ curve for pads 2 and 4_2 was still a nearly ideal rectifier. The localized nature of the switching demonstrates that one or more conductance channels such as those observed previously[2,32] penetrated the Schottky-like barrier under pad 4_1.

SWITCHING MECHANISM

On the basis of the experimental results from the thin-film and single-crystal devices, we propose a general model to explain the switching behaviour of the nanodevice in Fig. 1. The rectifying $I-V$ curve of the device in its virgin state (Fig. 1b) indicates that there are more oxygen vacancies at the bottom interface, and the

431

non-ohmic contact at the top interface dominates the electrical transport in the device. A negative voltage applied to the top electrode attracts positively charged vacancies in the oxide toward that electrode. The vacancy dopants drift in the electric field through the most favourable diffusion paths, such as grain boundaries, to form channels with a high electrical conductivity. Once one or more conductance channels penetrate the electronic barrier, the device is switched ON, producing a symmetric exponential $I-V$ that is the result of tunnelling through a thin residual barrier. In order to switch the device OFF, a voltage with the reverse polarity is applied. A positive bias on the top electrode repels the vacancies in the conducting channel away from the top interface and the original electronic barrier is recovered. The switching OFF is thus not the result of the rupture of a conducting filament by Joule heating (even though the process may be heat assisted), as proposed for models of unipolar switching[32], because it is bias-polarity dependent. It is crucial to note that the ON and OFF switching event occurs at one interface only: the rectifying non-ohmic (top) interface, not the ohmic-like (bottom) interface. The applied voltage bias may also alter the concentration of vacancies at the bottom interface, but this variation is not significant enough to change the ohmic contact property of that interface because (1) that interface has a very large concentration of vacancies, and (2) the electric field there is smaller due to the high conductivity. The non-ohmic interface has a very small concentration of vacancies, and is therefore sensitive to change, and sees a high electric field due to its low conductivity. The two interface junctions are in series, and in such deliberately asymmetric devices the total resistance is always controlled by the more resistive non-ohmic interface. The devices were also found to switch ON and OFF at lower voltages (for example, 0.1 V lower) than that shown in Fig. 1c, but with much longer time constants (hours), which is consistent with a slower nonlinear vacancy drift velocity under a lower electric field.

This model can be represented by an equivalent circuit for the device (top left inset, Fig. 1c), which comprises a rectifier in parallel with a memristor[33,34]. This switching model is fundamentally different from either the filamentary conduction model, which neglects the important role of the interface, or the modified Schottky barrier model, which assumes a uniform interfacial change. Instead, this model is inspired by the parallel conduction model[35,36], which posits that a macroscopic Schottky barrier is essentially a collection of a very large number of nanoscale diodes in parallel, with the net $I-V$ characteristic of the junction determined mainly by the diode with the lowest Schottky barrier height as long as it has a large enough cross-section such that it is not 'pinched off' by the potential of the surrounding material[37]. As native n-type dopants, a cluster of oxygen vacancies can significantly lower the local potential within the TiO$_2$. Under a negative bias, the vacancies drift toward the electronic barrier and form a conductive channel that shunts the rectifier. Coupled transport of charged dopants and electrons under a voltage bias that produces a switching effect has recently been shown to be the basis for the long-predicted memristor behaviour[34].

Using basic symmetry arguments, it was posited in 1971 (ref. 33) that a fourth fundamental passive circuit element must exist to complement the resistor, capacitor and inductor. Resistors-with-memory, or 'memristors' as they were termed, operate as dynamical resistors that change their state according to the time integral of applied current or voltage[33]. For our devices, the following equation describes the $I-V$ switching characteristic of the memristor + rectifier equivalent circuit shown in Fig. 1c:

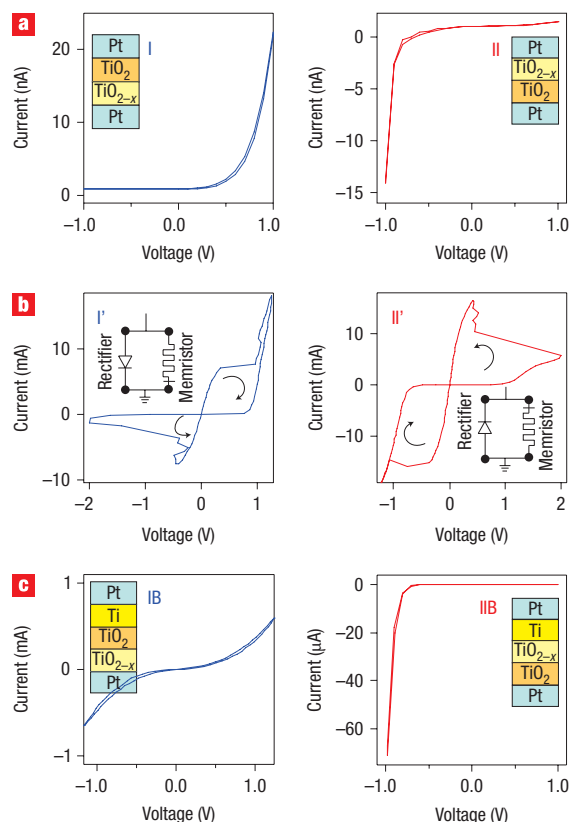$$I = w^n \beta \sinh(\alpha V) + \chi(\exp(\gamma V) - 1) \qquad (1)$$

Figure 4 Thin-film TiO$_{2-x}$ devices with controlled oxygen vacancy profiles verify the switching mechanism. a, Sample I and II with reversed layer sequences of 15-nm TiO$_2$ and 15-nm TiO$_{2-x}$ (more vacancies) layers show opposite polarities of $I-V$ curves in their virgin states. **b**, The switching polarities of these two samples are also opposite. **c**, Introducing more vacancies by adding a 5-nm Ti layer to the top interfaces of these two samples changes the $I-V$ curves in totally different ways, confirming the dominant role of the non-ohmic interfaces in the thin-film devices.

which was chosen more for its simplicity and ability to reproduce the $I-V$ behaviour than as a detailed physics model. In the first term, which represents a flux-controlled memristor[33], $\beta \sinh(\alpha V)$ is the approximation we use for the ON state of the memristor, which is essentially electron tunnelling through a thin residual barrier; α and β are fitting constants that are used to characterize the ON state, and w is the state variable of the memristor[34]. In this case w is proportional to the time integral of the voltage applied to the device (or, equivalently, the magnetic flux from Faraday's law of induction, although no extrinsic magnetic fields are involved here), and is normalized to have values between 0 (OFF) and 1 (ON). If $n = 1$, then the drift velocity of the oxygen vacancies is directly proportional to the applied electric field[34]. The second term in equation (1) represents the $I-V$ approximation for the rectifier, and χ and γ are the fitting constants used to characterize the net electronic barrier when the memristor is switched OFF. The exponent n of the state variable is used as a free parameter in the model, which we adjust to modify the switching between the ON and OFF states of the device to be consistent with the experimental observations. We find that the best agreement between our model and the measured switching characteristics (see Fig. 1c) occurs for n in the range from 14 to 22, which we interpret as evidence for a highly nonlinear dependence of the effective vacancy drift velocity on the voltage applied to the device.

According to our model, the rectification and switching polarities are both determined by the initial distribution of oxygen vacancies in the oxide layer. We tested this prediction by fabricating thin-film samples with engineered oxygen vacancy distributions. The oxide layers of these samples were actually bilayers of TiO_2 and TiO_{2-x} (containing a high concentration of vacancies) formed by intentionally creating one layer of oxide with a deficit of oxygen (see Methods). As shown in Fig. 4a, by reversing the fabrication sequence of the TiO_2 and TiO_{2-x} layers for samples I and II, we inverted both the rectification polarity of the virgin-state $I-V$ curves and simultaneously the polarity of the ON−OFF switching (Fig. 4b). Both results confirm the above switching model. In a second convincing test, an additional 5-nm Ti layer was interposed at the top interface of both samples to create yet more oxygen vacancies at this interface only. In Fig. 4c, we see that the virgin $I-V$ characteristics have been modified in opposite ways. As expected, sample IB became symmetric and very conductive (the current-limiting non-ohmic contact was reduced by the extra Ti). In contrast, sample IIB became even more rectifying (here the extra Ti created a better ohmic contact but did not affect the non-ohmic contact).

CONCLUSIONS

These experimental results establish that electrical conduction in metal/oxide/metal thin-film devices is controlled by a spatially heterogeneous metal/oxide electronic barrier. Memristive electrical switching proceeds by means of the drift of positively charged oxygen vacancies acting as native dopants to form (turn ON) or disperse (turn OFF) locally conductive channels through the electronic barrier. The location, concentration and distribution of oxygen vacancies in the as-fabricated TiO_2 film control the conductance, rectification and switching polarity of the device. We built TiO_2 crosspoints with engineered oxygen vacancy profiles that predictively control the switching polarity and conductance.

METHODS

The Pt and Ti metal layers were deposited by electron-beam evaporation at room temperature. The TiO_2 films were fabricated either by sputter deposition or atomic layer deposition (ALD) methods. The TiO_2 layer used for the junctions shown in Fig. 1 was 50 nm thick and was deposited by sputtering from a TiO_2 target with 3 mtorr Ar and 250 °C substrate temperature. The TiO_2 (15 nm)/TiO_{2-x} (15 nm) bilayer films used for the junctions shown in Fig. 4 were synthesized by ALD at 200 °C with an additional *in situ* annealing in a N_2 environment at 300 °C. The annealing process was carried out following the first 15-nm deposition to create oxygen vacancies in the lower half of the TiO_2 film, or was carried out following the full 30-nm deposition to create oxygen vacancies in the upper half of the TiO_2 film. Titanium (IV) isopropoxide precursor was used with water as the oxidizing agent for the ALD TiO_2 films. See Supplementary Information for detailed physical characterization of the TiO_2 single crystal and thin films; this includes infrared spectroscopy, Raman spectroscopy, X-ray diffraction, Rutherford backscattering spectroscopy, depth-profiled X-ray photoelectron spectroscopy, ultraviolet visible absorption spectroscopy, and electrical Hall effect measurements. The Ti (1.5-nm adhesion layer) + Pt (8-nm) electrode used for the 50 nm × 50 nm nanojunctions shown in Fig. 1 was patterned by ultraviolet-nanoimprint lithography. Details of the nanoimprint fabrication can be found in the references[26,27]. The Ti (5-nm adhesion layer) + Pt (15-nm) electrode used for the microjunctions (5 μm × 50 μm) shown in Fig. 4 was fabricated using a metal shadow mask. The single crystal TiO_2 rutile was a commercial single crystal (MTI Corporation). A single irreversible forming step was necessary for the as-prepared (virgin) devices before they exhibited repeatable switching cycles; for the nanodevices this forming occurred at approximately +8 V and 10 μA. An HP 4156 semiconductor parameter analyser was used for electrical characterization with the four-probe d.c. measurement method. The bottom electrodes of the junctions were grounded during all electrical measurements.

References

1. Vogel, E. M. Technology and metrology of new electronic materials and devices. *Nature Nanotech.* **2**, 25−32 (2007).
2. Szot, K. *et al.* Switching the electrical resistance of individual dislocations in single-crystalline $SrTiO_3$. *Nature Mater.* **5**, 312−320 (2006).
3. Aono, M. *et al.* Quantized conductance atomic switch. *Nature* **433**, 47−50 (2005).
4. Moore, G. E. Cramming more components onto integrated circuits. *Electronics* **38**, 114−116 (1965).
5. Mead, C. *Analog VLSI and Neural Systems* (Addison-Wesley, Reading, MA, 1989).
6. Boahen, K. Neuromorphic microchips. *Sci. Am.* **292**, 56−63 (2005).
7. Waser, R. & Aono, M. Nanoionics-based resistive switching memories. *Nature Mater.* **6**, 833−840 (2007).
8. Watanabe, Y. *et al.* Current-driven insulator−conductor transition and nonvolatile memory in chromium-doped $SrTiO_3$ single crystals. *Appl. Phys. Lett.* **78**, 3738−3740 (2001).
9. Chopra, K. L. Avalanche-induced negative resistance in thin oxide films. *J. Appl. Phys.* **36**, 184−187 (1965).
10. Simmons, J. G. & Verderber, R. R. New conduction and reversible memory phenomena in thin insulating films. *Proc. R. Soc. Lond. A* **301**, 77−102 (1967).
11. Rozenberg, M. J., Inoue, I. H. & Sánchez, M. J. Nonvolatile memory with multilevel switching: a basic model. *Phys. Rev. Lett.* **92**, 178302 (2004).
12. Chen, X., Wu, N., Strozier, J. & Ignatiev, A. Spatially extended nature of resistive switching in perovskite oxide thin films. *Appl. Phys. Lett.* **89**, 063507 (2006).
13. Fors, R., Khartsev, S. I. & Grishin, A. M. Giant resistance switching in metal−insulator−manganite junctions: evidence for Mott transition. *Phys. Rev. B* **71**, 045305 (2005).
14. Rohde, C. *et al.* Identification of a determining parameter for resistive switching of TiO_2 thin films. *Appl. Phys. Lett.* **86**, 262907 (2005).
15. Liu, S. Q.,Wu, N. J. & Ignatiev, A. Electric-pulse-induced reversible resistance change effect in magnetoresistive films. *Appl. Phys. Lett.* **76**, 2749−2751 (2000).
16. Nian, Y. B., Strozier, J., Wu, N. J., Chen, X. & Ignatiev, A. Evidence for an oxygen diffusion model for the electric pulse induced resistance change effect in transition-metal oxides. *Phys. Rev. Lett.* **98**, 146403 (2007).
17. Jeon, S. H., Park, B. H., Lee, J., Lee, B. & Han, S. First-principles modeling of resistance switching in perovskite oxide material. *Appl. Phys. Lett.* **89**, 042904 (2006).
18. Jameson, J. R. *et al.* Field-programmable rectification in rutile TiO_2 crystals. *Appl. Phys. Lett.* **91**, 112101 (2007).
19. Sawa, A., Fujii, T., Kawasaki, M. & Tokura, Y. Hysteretic current−voltage characteristics and resistance switching at a rectifying $Ti/Pr_{0.7}Ca_{0.3}MnO_3$ interface. *Appl. Phys. Lett.* **85**, 4073−4075 (2004).
20. Tsui, S., Wang, Y. Q., Xue, Y. Y. & Chu, C. W. Mechanism and scalability in resistive switching of metal−$Pr_{0.7}Ca_{0.3}MnO_3$ interface. *Appl. Phys. Lett.* **89**, 123502 (2006).
21. Baikalov, A. *et al.* Field-driven hysteretic and reversible resistive switch at the $Ag−Pr_{0.7}Ca_{0.3}MnO_3$ interface. *Appl. Phys. Lett.* **83**, 957−959 (2003).
22. Kim, K. M., Choi, B. J., Shin, Y. C., Choi, S. & Hwang, C. S. Anode-interface localized filamentary mechanism in resistive switching of TiO_2 thin films. *Appl. Phys. Lett.* **91**, 012907 (2007).
23. Fujii, T., Kawasaki, M., Sawa, A. & Akoh, H. Hysteretic current−voltage characteristics and resistance switching at an epitaxial oxide Schottky junction $SrRuO_3/SrTi_{0.99}Nb_{0.01}O_3$. *Appl. Phys. Lett.* **86**, 012107 (2005).
24. Tsunoda, K. *et al.* Bipolar resistive switching in polycrystalline TiO_2 films. *Appl. Phys. Lett.* **90**, 113501 (2007).
25. Lee, D. *et al.* Resistance switching of copper doped MoO_x films for nonvolatile memory applications. *Appl. Phys. Lett.* **90**, 122104 (2007).
26. Jung, G. Y. *et al.* Fabrication of a 34 × 34 crossbar structure at 50 nm half-pitch by UV-based nanoimprint lithography. *Nano Lett.* **4**, 1225−1229 (2004).
27. Jung, G. Y. *et al.* Circuit fabrication at 17 nm half-pitch by nanoimprint lithography. *Nano Lett.* **6**, 351−354 (2006).
28. Szot, K., Speier, W. & Eberhardt, W. Microscopic nature of the metal to insulator phase transition induced through electroreduction in single-crystal $KNbO_3$. *Appl. Phys. Lett.* **60**, 1190−1192 (1992).
29. Knauth, P. & Tuller, H. L. Electrical and defect thermodynamic properties of nanocrystalline titanium dioxide. *J. Appl. Phys.* **85**, 897−902 (1999).
30. Rhoderick, E. H. & Williams, R. H. *Metal−Semiconductor Contacts*, 2nd edn (Oxford Science Publications, Oxford 1988).
31. Weibel, A., Bouchet, R. & Knauth, P. Electrical properties and defect chemistry of anatase (TiO_2). *Solid State Ionics* **177**, 229−236 (2006).
32. Choi, B. J. *et al.* Resistive switching mechanism of TiO_2 thin films grown by atomic-layer deposition. *J. Appl. Phys.* **98**, 033715 (2005).
33. Chua, L. O. Memristor — missing circuit element. *IEEE Trans. Circuit Theory* **CT-18**, 507−519 (1971).
34. Strukov, D. B., Snider, G. S., Stewart, D. R. & Williams, R. S. The missing memristor found. *Nature* **453**, 80−83 (2008).
35. Ohdomari, I. & Tu, K. N. Parallel silicide contacts. *J. Appl. Phys.* **51**, 3735−3739 (1980).
36. Tung, R. T. Electron transport at metal−semiconductor interfaces: General theory. *Phys. Rev. B* **45**, 13509−13523 (1992).
37. Talin, A. A., Williams, R. S., Morgan, B. A., Ring, K. M. & Kavanagh, K. L. Nanometer-resolved spatial variations in the Schottky barrier height of a Au/n-type GaAs diode. *Phys. Rev. B* **49**, 16474−16479 (1994).